Rare Metal Materials and Engineering
Volume 53, Issue 5, May 2024
Available online at www.rmme.ac.cn

Science Press

Cite this article as: Liu Meijun, Xu Liujie, Li Zhou, et al. Microstructure and Wear Properties of WMoNbTaV-Al_2O_3 High Entropy Alloy Prepared by Spark Plasma Sintering[J]. Rare Metal Materials and Engineering, 2024, 53(05): 1236-1244. DOI: 10.12442/j.issn.1002-185X.20230049.

ARTICLE

Microstructure and Wear Properties of WMoNbTaV-Al_2O_3 High Entropy Alloy Prepared by Spark Plasma Sintering

Liu Meijun[1], Xu Liujie[1,2], Li Zhou[1], Guo Mingyi[1], Hu Jikang[1], Shen Huahai[3]

[1] School of Materials Science and Engineering, Henan University of Science and Technology, Luoyang 471000, China; [2] Henan International Joint Laboratory for High Temperature Refractory Metal Materials, Henan University of Science and Technology, Luoyang 471000, China; [3] Institute of Nuclear Physics and Chemistry, China Academy of Engineering Physics, Mianyang 621900, China

Abstract: A new refractory high entropy alloy WMoNbTaV containing Al_2O_3 was prepared by spark plasma sintering. The effects of sintering temperature on densification behavior, phase structure, microstructure and wear resistance of the alloy were studied. The results show that when sintered at 1800–1900 °C, the matrix of WMoNbTaV-Al_2O_3 has a single bcc phase structure, and the average grain size of Al_2O_3 is 1.15 μm. With the increase in sintering temperature, the grain size of the alloy increases, the density and microhardness also increase, and the hardness reaches 7967.4 MPa when the sintering temperature is 1900 °C. The alloy sintered at 1900 °C has excellent wear resistance, and the wear amount is only half of that of the alloy sintered at 1800 °C. The wear resistance of WMoNbTaV-Al_2O_3 high entropy alloy is much higher than that of pure W material. When the abrasive particle size is 37.5 μm, the wear mass loss of alloy sintered at 1900 °C is 0.9 mg, and the wear resistance of alloy is 83 times higher than that of pure W material.

Key words: spark plasma sintering; refractory high entropy alloy; microstructure; wear

Since the proposal of refractory high entropy alloys in 2010, numerous scholars have shown great interest in their properties, making them a significant focal point in the field of high entropy alloy research. Refractory high entropy alloys exhibit exceptional mechanical properties, wear resistance, corrosion resistance, physical properties and high temperature properties (including high temperature strength, high temperature phase stability, high temperature oxidation resistance, etc) [1–5]. The excellent properties of refractory high entropy alloys make them expected to become potential materials in various fields such as high-temperature/nuclear structural material, high-temperature thermoelectric materials and new magnetic material. These alloys have broad application prospects and research value in aerospace, nuclear energy, superconductor, electronic chemical industry and other fields[6–10].

Due to the characteristics of fast heating rate, short sintering time, small sintered grains and uniform composition, spark plasma sintering has been increasingly utilized in the preparation of refractory high entropy alloys[11–15]. According to the Hall-Petch formula, the finer the grains, the higher the yield strength, and the more significant the crystal strengthening. Therefore, the mechanical properties of refractory high entropy alloy prepared by the spark plasma sintering method were found to be more excellent[16–17]. Naser-Zoshki et al[18] prepared $W_{10}Mo_{27}Cr_{21}Ti_{22}Al_{20}$ refractory high entropy alloy through mechanical alloying and spark plasma sintering. This alloy exhibits better high temperature specific strength compared to traditional nickel-based superalloys and most reported refractory high entropy alloys, making it a promising candidate for high temperature applications. Zhu et al[19] prepared TiZrNbMoTa refractory high entropy alloy by mechanical alloying and spark plasma sintering. They discovered that this alloy demonstrates superior mechanical properties compared with the as-cast alloy prepared by arc melting.

The sintering process plays a crucial role in determining the properties of cemented carbide. Sintering temperature[20–24], sintering pressure[25–27] and holding time[28–30] are key factors that influence the preparation of refractory high entropy alloy by spark plasma sintering. The impact of sintering

Received date: November 14, 2023
Foundation item: National Natural Science Foundation of China (U2004180); National Key R&D Program of China (2020YFB2008400)
Corresponding author: Xu Liujie, Ph. D., Professor, Henan International Joint Laboratory for High Temperature Refractory Metal Materials, Henan University of Science and Technology, Luoyang 471000, P. R. China, E-mail: xlj@haust.edu.cn

temperature on the properties of refractory high entropy alloys is significant, but the findings are not consistent. Some researchers[27–28,31] argue that increasing the sintering temperature leads to larger grain sizes in high entropy alloys, resulting in increased density, hardness and yield strength. However, Long et al[25] found that as the sintering temperature rises, the proportion of twin boundaries increases, leading to a decrease in the hardness and yield strength of $Fe_{50}Mn_{30}Co_{10}Cr_{10}$ high entropy alloy. Yan et al[32] also found that too high sintering temperature enhances the dissolution of the second phase, reduces the amount and size of precipitated phase, and gradually diminishes the hardness of NbMoCrTiAl high entropy alloy. Consequently, it is crucial to identify the appropriate sintering temperature and holding time for producing refractory high entropy alloys with exceptional comprehensive properties.

The addition of α-Al_2O_3 to the metal can greatly improve the mechanical properties of the material, both at room temperature and high temperature. These improvements include increased tensile strength, yield strength and hardness[33]. Wang et al[34] found that the HfNbTaTiZrV refractory high entropy alloy, enhanced by the addition of Al_2O_3, demonstrates an increase in yield strength. This increase can be attributed to the combined effects of multiple strengthening mechanisms, such as solid solution strengthening, gap strengthening, grain boundary strengthening and dispersion strengthening. Raghavendra et al[35] electrodeposited Ni and Ni-α-Al_2O_3 nanocomposite coatings on Al6061 matrix, and found that the wear rate of the Ni-Al_2O_3 composite coating is lower than that of the Ni coating. This is attributed to the presence of α-Al_2O_3 particles, which restrict the movement of dislocations.

In this work, a new type of high entropy alloy WMoNbTaV containing α-Al_2O_3 was prepared by spark plasma sintering using mixed metal powder as raw material. The effects of different sintering temperatures (1800, 1850, 1900 °C) on the microstructure, microhardness and wear properties of the WMoNbTaV-Al_2O_3 high entropy alloy were investigated, and the wear mechanism was discussed. The main objective of this research is to achieve a WMoNbTaV-Al_2O_3 high entropy alloy with favorable wear properties by controlling the temperature during spark plasma sintering. The experimental findings and theoretical insights provided in this study contribute to the advancement in high performance of high entropy alloy materials via powder metallurgy.

1 Experiment

A new high entropy alloy of WMoNbTaV containing Al_2O_3 was designed. The powders of W, Mo, Nb, Ta, V with a purity of 99.99% and a particle size of approximately 10 μm and Al_2O_3 powders were selected as raw materials. The powders were mixed in an equal molar ratio of W, Mo, Nb, Ta, V, and 1wt% Al_2O_3. Tungsten carbide balls were used as the grinding medium, and ball milling was conducted at a speed of 150 r/min for 70 h. The resulting ball milling diagram of the mixed powder is shown in Fig. 1a, and the mixed powder of WMoNbTaV-Al_2O_3 high entropy alloy was obtained.

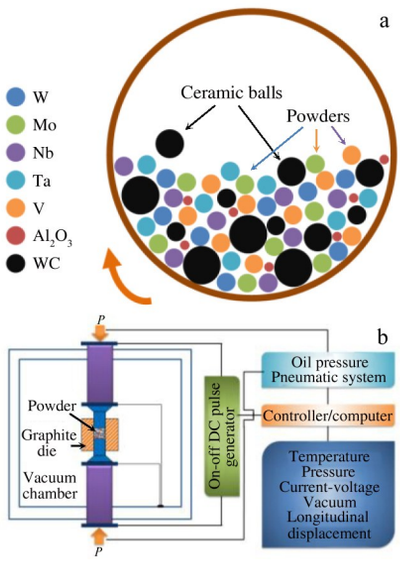

Fig.1 Schematic diagrams of ball milling mixing (a) and spark plasma sintering (b) for WMoNbTaV-Al_2O_3 high entropy alloy

To pressurize the WMoNbTaV-Al_2O_3 high entropy alloy powder mixture, a spark plasma sintering furnace (20T-10) was employed, as depicted in Fig. 1b. The mixed powder was compacted at a pressure of 30 MPa under vacuum condition (2×10^{-2} Pa). It was then heated to 600 °C at a rate of 120 °C/min, followed by raising the temperature to the sintering temperature (1800, 1850, 1900 ° C) at a rate of 100 ° C/min. The mixture was held at the sintering temperature for 10 min and subsequently cooled in the furnace. Finally, a sintered cylinder with 20 mm in diameter and 6 mm in height was prepared.

The crystal structure of the WMoNbTaV-Al_2O_3 high entropy alloy was analyzed by X-ray diffraction (XRD, Brux-D8). The microstructure and elemental composition of the WMoNbTaV- Al_2O_3 high entropy alloy were characterized by field emission scanning electron microscopy (SEM) and energy dispersive spectroscopy (EDS). The grain size and orientation of the WMoNbTaV-Al_2O_3 high entropy alloy were determined by electron backscattered diffraction (EBSD, Oxford C-nano). Square samples of the high entropy alloy measuring 2 mm×5 mm×8 mm were cut and then polished. After ultrasonic cleaning, an argon ion cross-section polishing machine (CP, JEOL IB-19530) was used for ion polishing. The polishing process lasted for 20 min with a voltage of 7.5 kV and a constant current of approximately 120 μA. Finally, EBSD samples were prepared.

The density of sintered samples of WMoNbTaV-Al_2O_3 high entropy alloy was measured by density measuring instrument (ME203/02). The polished sintered sample was tested by microhardness tester (HVS-1000) under a loading of 4.9 N and a residence time of 10 s. At least 10 different domains of each sample were randomly tested to obtain an average density value.

The wear performance of sintered WMoNbTaV-Al_2O_3

refractory high entropy alloy samples was evaluated using a wear testing machine (ML-100 model), as shown in Fig.2. The wear test was conducted under a pressure of 1.41 MPa, and the testing machine disc was rotated at a speed of 60 r/min. The test samples had a size of Φ3 mm×6 mm. The sintered sample was moved 10 times between the center and the edge of the disc at a speed of 2.5 mm/s, following a spiral path. The wear properties of sintered WMoNbTaV-Al_2O_3 high entropy alloy samples were compared by alumina abrasive paper with different sizes (12.5, 18.75, 37.5, 100 μm). Three sets of repeated tests were conducted for each sample, and the average grinding mass loss was calculated.

2 Results and Discussion

2.1 Phase composition of WMoNbTaV-Al_2O_3 high entropy alloy

Fig.3 presents the XRD patterns of WMoNbTaV-Al_2O_3 high entropy alloy sintered at 1800, 1850 and 1900 °C. In the 20°–90° range, four characteristic peaks corresponding to (110), (200), (211) and (220) crystal faces are observed at 39.8°, 57.7°, 72.5° and 86.1°, respectively. These peaks indicate the occurrence of diffusion and solid solution between components, resulting in the formation of a solid solution. The phase composition of the high entropy alloy powder remains consistent after sintering at different temperatures, suggesting that the sintering temperature has no significant impact on the phase structure of the WMoNbTaV-Al_2O_3 high entropy alloy. The strong peak position of the diffraction pattern indicates an increase in peak intensity and a decrease in peak width, confirming the presence of a similar single body centered cubic (bcc) phase structure. Consequently, it can be concluded that the WMoNbTaV-Al_2O_3 high entropy alloy matrix, regardless of the sintering temperature, exhibits a single disordered bcc solid solution phase.

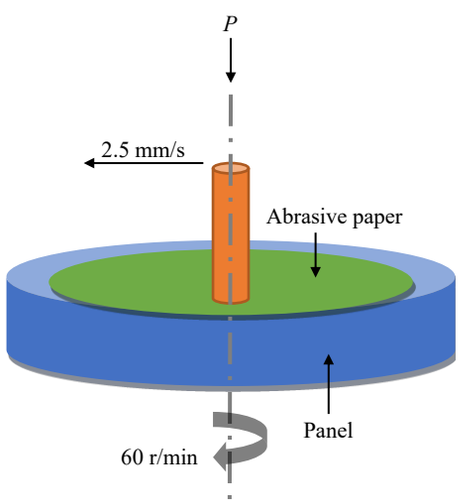

Fig.2 Schematic diagram of abrasive wear test

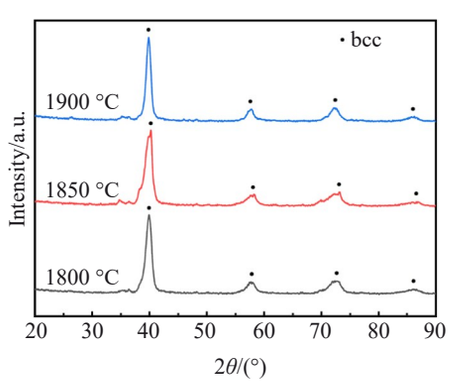

Fig.3 XRD patterns of WMoNbTaV-Al_2O_3 high entropy alloy at different sintering temperatures

2.2 Microstructure of WMoNbTaV-Al_2O_3 high entropy alloy

SEM-EDS analysis of the WMoNbTaV-Al_2O_3 high entropy alloy microstructure was conducted at various sintering temperatures, as shown in Fig. 4. The results reveal that the sintered alloy consists of continuous matrix and Al_2O_3 phase. The black area corresponds to the alumina phase, the gray-black area represents the pits left by the shedding of alumina, and the continuous gray area indicates the high entropy alloy matrix. In Fig.4a, numerous pits formed by Al_2O_3 shedding are observed, and the Al_2O_3 phase becomes coarse and irregular. However, in Fig. 4c, the shedding pits of Al_2O_3 are hardly visible, and the Al_2O_3 phase exhibits a nearly spherical shape. The presence of spherical alumina with lower interfacial energy contributes to reduction in system free energy and enhances the overall stability of the alloy microstructure.

According to the EDS analysis, when the sintering temperature is 1800 °C, the elements of the high entropy alloy exhibit partial segregation. However, at sintering temperature of 1900 °C, the segregation of elements is greatly weakened, resulting in a more uniform distribution. This improvement is attributed to the higher sintering temperature, which provides sufficient energy for the complete diffusion between the atoms of each element[19], thereby accelerating the atomic diffusion rate and enhancing the uniformity of element distribution. As the sintering temperature increases, the microstructure of the alloy becomes more uniform, the alumina particles tend to be spherical, and the matrix exhibits a stronger bond.

Fig.5 presents the EBSD results of WMoNbTaV-Al_2O_3 high entropy alloy at different sintering temperatures. The impact of sintering temperature on grain size is determined. As shown in Fig. 5, the average grain size of the high entropy alloy increases from 4.18 μm at 1800 °C to 7.12 μm at 1850 °C, and further increases to 8.95 μm at 1900 °C. The accelerated grain boundary migration rate and grain growth caused by high temperature sintering lead to an increase in grain size. The grain size of the alloy matrix phase gradually increases from 4.18 μm to 7.14 μm and then to 9.05 μm. In contrast, the grain size of the Al_2O_3 phase is approximately 1.15 μm. The dispersion of Al_2O_3 particles within the matrix hinders the migration of grain boundaries, resulting in less noticeable grain growth. Therefore, the grain size of the alloy exhibits a

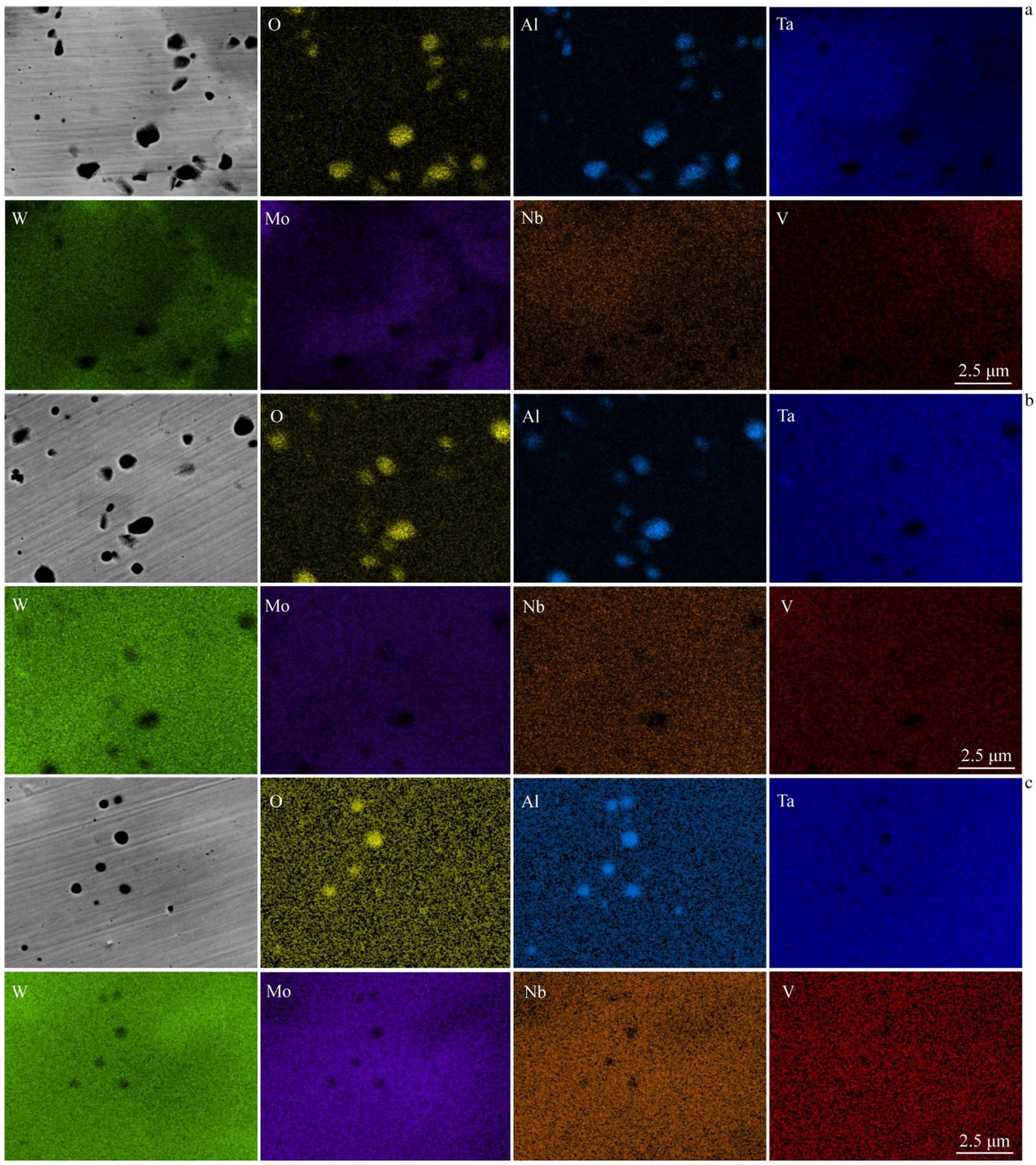

Fig.4 SEM-EDS results of WMoNbTaV-Al_2O_3 high entropy alloy at different sintering temperatures: (a) 1800 °C, (b) 1850 °C, and (c) 1900 °C

slow increase with sintering temperature[36].

2.3 Physical properties of WMoNbTaV-Al_2O_3 high entropy alloy

The density of the WMoNbTaV-Al_2O_3 high entropy alloy is determined by Archimedes drainage method. The relative density (ε) can be calculated by following formula:

$$\varepsilon = \rho/\rho_0 \quad (1)$$

where ρ is the measured density and ρ_0 is the theoretical density which is found to be 12.096 g/cm^3. During the sintering process, the density of the alloy increases from 11.546 g/cm^3 at 1800 °C to 11.568 g/cm^3 at 1850 °C, and with further increasing the sintering temperature to 1900 °C, it rises to 11.682 g/cm^3. The densification degree of the alloy at different sintering temperatures exceeds 95%, and higher temperatures lead to higher densification degree. The intense melting of alloy particles and filling of pores are facilitated by the discharge plasma produced during high temperature sintering, resulting in a reduction in pores and higher density

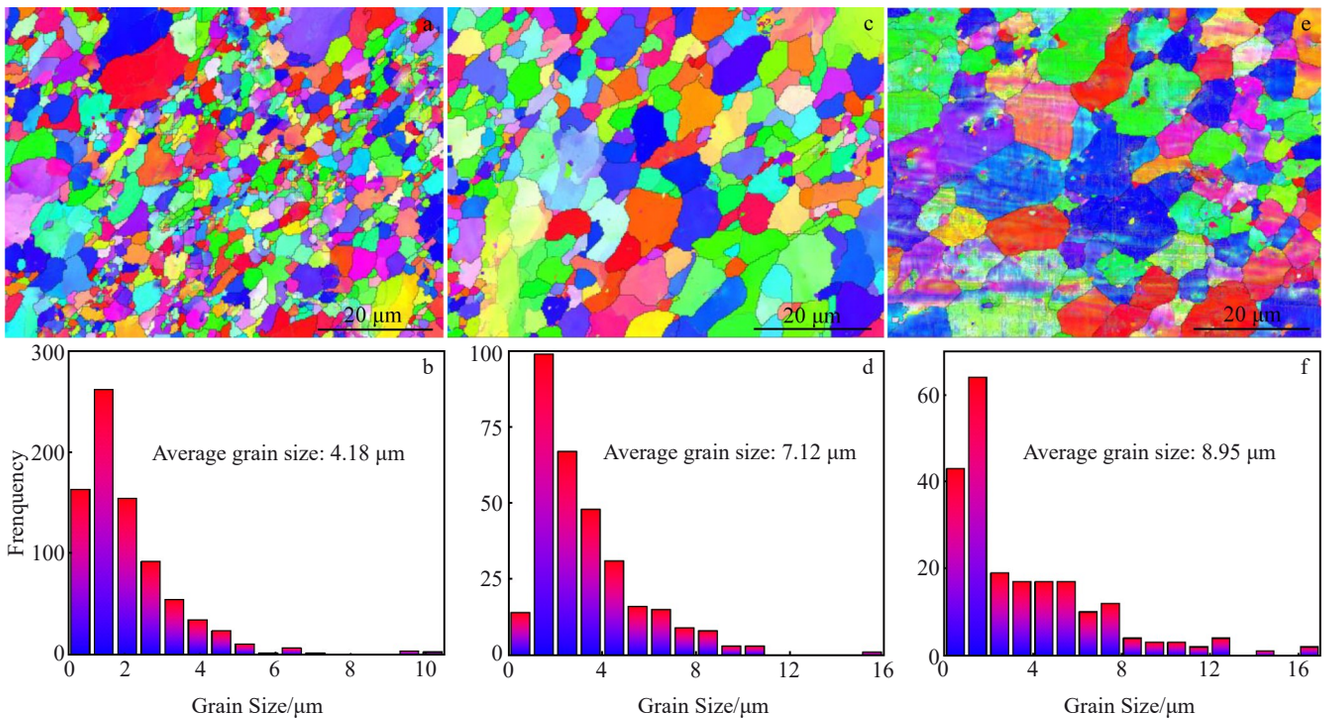

Fig.5 EBSD results of WMoNbTaV-Al_2O_3 high entropy alloy sintered at different temperatures (a, c, e) and corresponding grain size distributions (b, d, f): (a–b) 1800 °C, (c–d) 1850 °C, and (e–f) 1900 °C

of the alloy.

Table 1 shows the physical properties of WMoNbTaV-Al_2O_3 high entropy alloy sintered at different temperatures. It is evident that the microhardness of the high entropy alloy remarkably increases with the rise in sintering temperature. The average microhardness values for WMoNbTaV-Al_2O_3 alloy at 1800, 1850 and 1900 ° C are 5478.2, 6095.6 and 7967.4 MPa, respectively. As the sintering temperature increases, the number of micropores in the alloy decreases, leading to an increase in hardness. The higher sintering temperature also results in higher density, which further contributes to the improvement in hardness. Moreover, the increase in sintering temperature can intensify the lattice deformation caused by the diffusion of elements with different atomic radii, thereby enhancing atomic movement, promoting grain boundary pinning, and ultimately leading to an improvement in alloy hardness. The sintered WMoNbTaV-Al_2O_3 alloy in this study exhibits significantly superior properties compared with most reported refractory high entropy alloys[37–45] prepared by casting or powder metallurgy, as depicted in Fig.6. The small error bars in the figure indicate a highly uniform structure and stable performance of the alloy.

Table 1 Physical properties of WMoNbTaV-Al_2O_3 high entropy alloy sintered at different temperatures

Sintering temperature/°C	Density/ g·cm^{-3}	Consistency /%	Microhardness, HV/MPa
1800	11.546	95.45	5478.2
1850	11.568	95.63	6095.6
1900	11.682	96.58	7967.4

2.4 Wear properties of WMoNbTaV-Al_2O_3 high entropy alloy

Fig. 7 shows the wear test results of WMoNbTaV-Al_2O_3 high entropy alloy sintered at different temperatures. The wear resistance is expressed by the process parameter ε ($\varepsilon = W_0/W$, where W_0 represents the wear mass loss of pure tungsten and W is the wear mass loss of high entropy alloy). From Fig. 7a, the wear resistance of the alloy increases with the rise in sintering temperature, under the same particle size conditions. When the abrasive particle size is 100 μm, the wear mass loss of the alloy sintered at 1900 °C is approximately half of that of the alloy sintered at 1800 ° C, indicating better wear resistance. Moreover, the wear behavior of the WMoNbTaV-

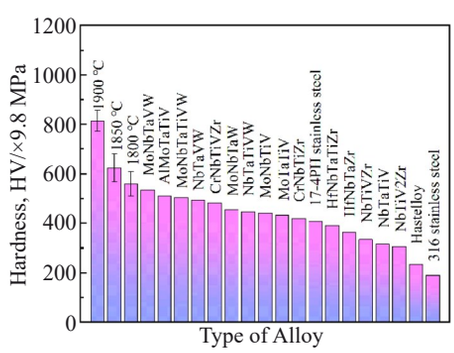

Fig.6 Comparison of hardness of different refractory high entropy alloys

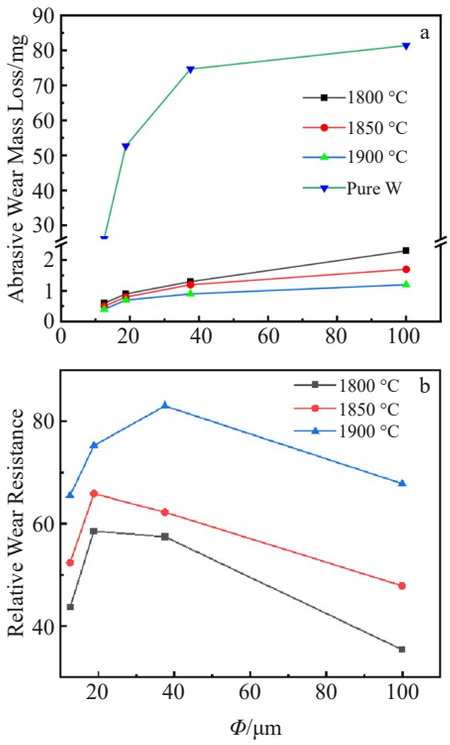

Fig.7 Wear test results of WMoNbTaV-Al_2O_3 high entropy alloy with different abrasive particle sizes and sintering temperatures: (a) mass loss of abrasive wear and (b) relative wear resistance

Al_2O_3 high entropy alloy is also influenced by the particle size at a given sintering temperature. Specifically, as the abrasive particle size increases from 12.5 μm to 100 μm, the abrasive wear mass loss of the alloy sintered at 1900 °C increases from 0.4 mg to 1.2 mg, representing a threefold increase.

Comparing Fig.7a and 7b, it can be observed that the wear resistance of WMoNbTaV-Al_2O_3 high entropy alloy is significantly higher than that of pure W material under the same wear conditions. When the abrasive particle size is 37.5 μm, the wear amount of the alloy sintered at 1900 °C is 0.9 mg, indicating a relative wear resistance that is 83 times higher than that of pure W material. Similarly, when the abrasive particle size is 18.75 μm, the mass loss of the alloy sintered at 1800 and 1850 °C alloy is 0.9 and 0.8 mg, respectively, suggesting the relative wear resistances that are 58.6 and 65.9 times higher than that of pure W material.

This study reveals a positive correlation between the wear resistance of WMoNbTaV-Al_2O_3 high entropy alloy and the sintering temperature, as well as negative correlation with the abrasive particle size. Specifically, an increase in abrasive particle size leads to an increase in abrasive wear mass loss and a decrease in the wear resistance of WMoNbTaV-Al_2O_3 high entropy alloy at a constant sintering temperature. Furthermore, under the same particle size, higher sintering temperatures result in smaller abrasive wear mass loss and improved wear resistance of WMoNbTaV-Al_2O_3 high entropy alloy, which is consistent with the trend observed in microhardness.

2.5 Wear mechanism of WMoNbTaV-Al_2O_3 high entropy alloy

The wear morphology of pure W material is examined under different particle sizes, as shown in Fig. 8. As the abrasive particle size increases, the number of grooves on the material's surface also increases. Additionally, the wear marks are deepened and widened, indicating an increase in the wear degree. When the particle size is 100 μm, the wear surface of pure W material exhibits a spalling lamellar structure and spalling pits caused by fatigue spalling. Fig. 8d clearly shows that the wear degree of pure W material is more severe, indicating poor wear resistance. The wear surface of pure W material displays a series of deep grooves parallel to the sliding direction, suggesting that the wear mechanism involves abrasive wear accompanied by slight plastic deformation.

The results from Fig. 9 – Fig. 11 demonstrate that as the sintering temperature increases, the wear scratches on the alloy decrease and the surfaces become smoother. This indicates that the wear mechanism of the WMoNbTaV-Al_2O_3 high entropy alloy is not affected by the sintering temperature, but rather the degree of wear. Specifically, when the particle size is 12.5 μm, the wear surface of the alloy sintered at 1900 °C is extremely smooth with minimal scratches. Furthermore, when the particle size increases to 18.75 μm, the wear surface of the alloy remains relatively smooth with some shallow furrows, suggesting a typical mild wear mechanism. As the abrasive size further increases, the wear surface of the alloy is deepened gradually, and the number of furrows increases to cover the entire wear area. The furrow spacing on the wear marks of the WMoNbTaV-Al_2O_3 high entropy alloy is fine and the surface remains smooth. There is no layer structure on the edge of the furrow, and only a small amount of oxide is observed on the surface. The plastic deformation is uniformly distributed and no cracks are formed. Therefore, the

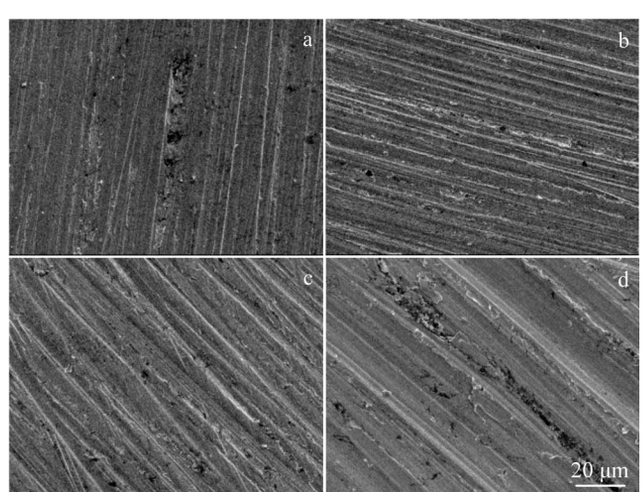

Fig.8 Wear morphologies of pure W material with different abrasive particle sizes: (a) 12.5 μm, (b) 18.75 μm, (c) 37.5 μm, and (d)100 μm

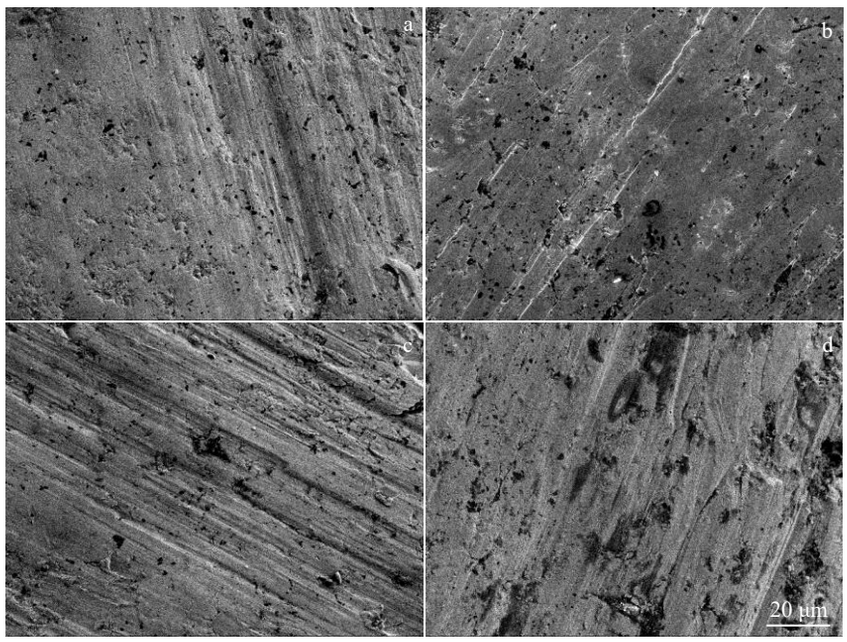

Fig.9 Wear morphologies of WMoNbTaV-Al_2O_3 high entropy alloy sintered at 1800 °C with different abrasive particle sizes: (a) 12.5 μm, (b) 18.75 μm, (c) 37.5 μm, and (d) 100 μm

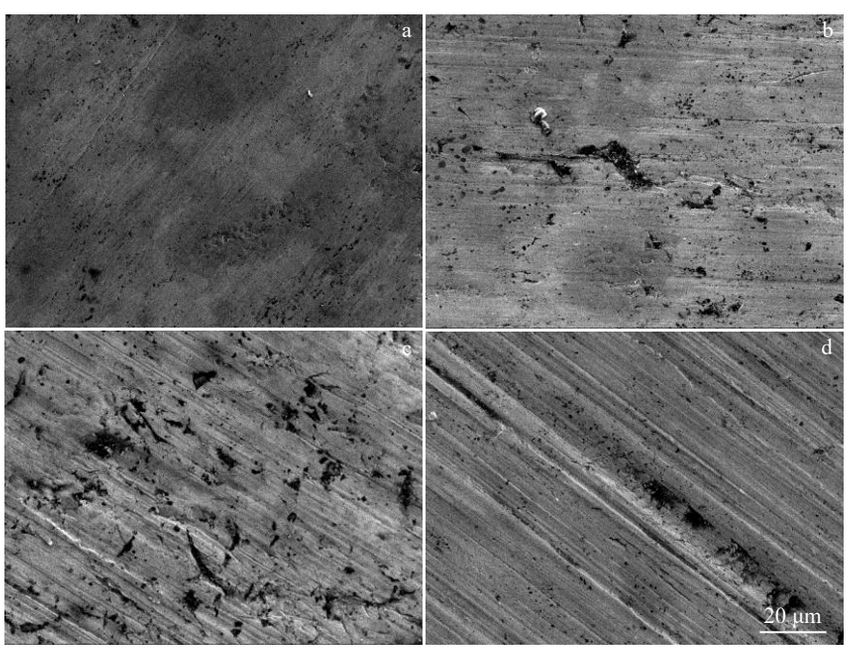

Fig.10 Wear morphologies of WMoNbTaV-Al_2O_3 high entropy alloy sintered at 1850 °C with different abrasive particle sizes: (a) 12.5 μm, (b) 18.75 μm, (c) 37.5 μm, and (d) 100 μm

main wear mechanism of the WMoNbTaV-Al_2O_3 high entropy alloy is identified as abrasive wear.

Comparing Fig. 8 – Fig. 11, it can be observed that the grooves formed by abrasive wear in pure W material are relatively deep and have obvious layer structure, while the surface grooves of WMoNbTaV-Al_2O_3 high entropy alloy are relatively shallow. The wear resistance of WMoNbTaV-Al_2O_3 high entropy alloy is found to be superior to that of pure W material due to the following reasons.

(1) The hardness of WMoNbTaV-Al_2O_3 high entropy alloy is significantly higher than that of pure W material. According to the classic Archard law, higher hardness in alloy translates to better wear resistance.

(2) The presence of Al_2O_3 phase in WMoNbTaV-Al_2O_3 high entropy alloy contributes to improved wear resistance. The Al_2O_3 phase not only exhibits high hardness, but also possesses good toughness. Moreover, the Al_2O_3 phase is dispersed within the matrix, enabling the alloy to effectively

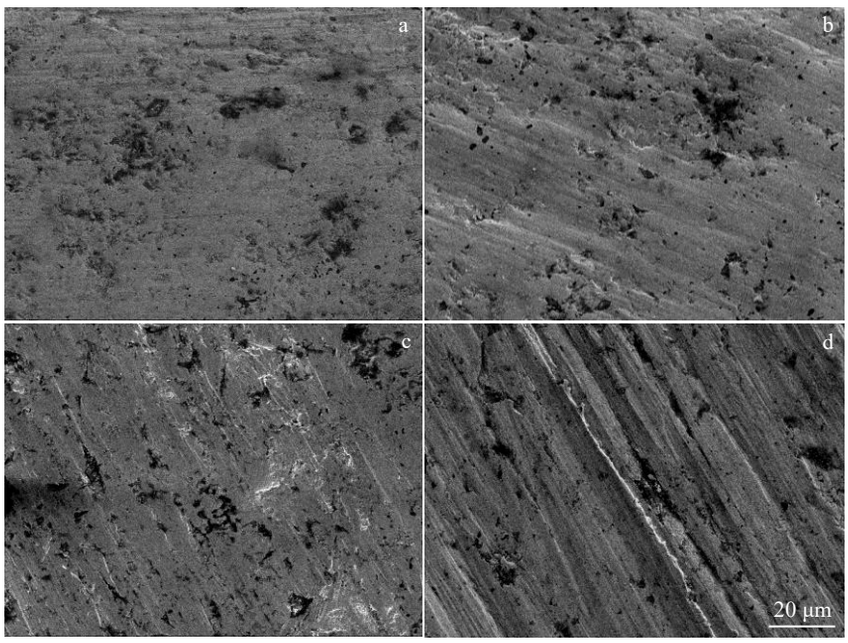

Fig.11 Wear morphologies of WMoNbTaV-Al_2O_3 high entropy alloy sintered at 1900 °C with different abrasive particle sizes: (a) 12.5 μm, (b) 18.75 μm, (c) 37.5 μm, and (d)100 μm

resist abrasion scratches, and providing excellent softening resistance[46–47].

(3) The wear mechanism observed in WMoNbTaV-Al_2O_3 high entropy alloy is primarily abrasive wear, while the wear surface of pure W material exhibits slight plastic deformation alongside abrasive wear. This results in the formation of large-sized abrasive particles, intensifying the wear on the pure W surface. Therefore, it can be concluded that WMoNbTaV-Al_2O_3 high entropy alloy demonstrates exceptional wear resistance based on the wear morphology observed.

3 Conclusions

1) The spark plasma sintered WMoNbTaV-Al_2O_3 high entropy alloy matrix consists of a single bcc phase. As the sintering temperature increases, average grain size, density and microhardness of the alloy also increase. At a sintering temperature of 1900 °C, the alloy exhibits an average grain size of 8.95 μm, a density of 96.58%, and a microhardness of 7967.4 MPa.

2) When subjected to the same wear conditions, the WMoNbTaV-Al_2O_3 high entropy alloy demonstrates significantly higher wear resistance than pure W material. At an abrasive particle size of 37.5 μm, the alloy experiences a wear mass loss of 0.9 mg at 1900 °C, which is 83 times higher than that of pure W material. The wear mechanism of pure W material involves abrasive wear accompanied by slight plastic deformation, whereas the wear mechanism of the WMoNbTaV-Al_2O_3 high entropy alloy is primarily abrasive wear.

3) The wear resistance of the WMoNbTaV-Al_2O_3 high entropy alloy exhibits a positive correlation with sintering temperature and a negative correlation with wear particle size. With increasing the sintering temperature, the hardness is improved and the abrasive wear mass loss decreases, resulting in improved wear resistance of the WMoNbTaV-Al_2O_3 high entropy alloy. The alloys sintered at 1800 and 1850 °C are suitable for fine abrasive wear conditions, while the alloy sintered at 1900 °C is appropriate for medium abrasive wear conditions.

References

1 Ren X, Li Y, Qi Y *et al. Materials*[J], 2022, 15(8): 2931
2 Tian Y S, Zhou W Z, Tan Q B *et al. Transactions of Nonferrous Metals Society of China*[J], 2022, 32(11): 3487
3 Hua X J, Hu P, Xing H R *et al. Acta Metallurgica Sinica (English Letters)*[J], 2022, 35(8): 1231
4 Yan Y G, Lu D, Wang K. *Tungsten*[J], 2023, 5(1): 32
5 Zhu C, Xu L, Liu M *et al. Journal of Materials Research and Technology*[J], 2023, 24: 7832
6 Jiang X, Chen L, Hao X H *et al. Journal of Materials Engineering*[J], 2022, 50(3): 33
7 Ding Hongyu, Yin Yanjun, Guan Jieren *et al. Rare Metal Materials and Engineering*[J], 2021, 50(6): 2237 (in Chinese)
8 Yan Y G, Wang K. *Tungsten*[J], 2023, 5(4): 531
9 Li Tianxin, Lu Yiping, Cao Zhiqiang *et al. Acta Metallurgica Sinica*[J], 2021, 57 (1): 42 (in Chinese)
10 Zhang Ping, Jiang Lin, Yang Jinxue *et al. Materials Reports*[J], 2022, 36(14): 5 (in Chinese)
11 Wei Y G, Guo G, Li J *et al. Journal of Aeronautical Materials*[J], 2019, 39(5): 12
12 Xiong W, Guo A X Y, Liu C T *et al. Journal of Materials Science & Technology*[J], 2023, 142: 196
13 Srikanth M, Annamalai A R, Muthuchamy A *et al. Crystals*[J],

2021, 11(6): 612
14 Fu A, Guo W, Liu B *et al. Journal of Alloys and Compounds*[J], 202, 815: 152466
15 Lv S S, Zu Y F, Chen G Q *et al. Materials Science and Engineering A*[J], 2020, 795: 140035
16 Xu Liujie, Zong Le, Luo Chunyang *et al. Acta Metallurgica Sinica*[J], 2022, 58(3): 257 (in Chinese)
17 Zong Le, Xu Liujie, Luo Chunyang *et al. Chinese Journal of Engineering*[J], 2021, 43(11): 1459 (in Chinese)
18 Naser-Zoshki H, Kiani-Rashid A R, Vahdati-Khaki J. *Proceedings of the Institution of Mechanical Engineers, Part L: Journal of Materials: Design and Applications*[J], 2022, 236(4): 695
19 Zhu C, Li Z, Hong C *et al. International Journal of Refractory Metals and Hard Materials*[J], 2020, 93: 105357
20 Zhu Dezhi, Wu Jipeng, Liu Shiwen. *Rare Metal Materials and Engineering*[J], 2020, 49(11): 3875 (in Chinese)
21 Alcalá M D, Real C, Fombella I *et al. Journal of Alloys and Compounds*[J], 2018, 749: 834
22 Gao Nan, Long Yan, Peng Haiyan *et al. Chinese Journal of Materials Research*[J], 2019, 33(8): 572 (in Chinese)
23 Ujah C O, Popoola A P I, Popoola O M *et al. Journal of Materials Engineering and Performance*[J], 2023, 32(1): 18
24 Alcalá M D, Real C, Fombella I *et al. Journal of Alloys and Compounds*[J], 2018, 749: 834
25 Long Yan, Peng Liang, Zhang Weihua *et al. Chinese Journal of Rare Metals*[J], 2021, 45(7): 769 (in Chinese)
26 Liu Jia, An Xuguang, Kong Qingquan *et al. Journal of Chengdu University (Natural Science)*[J], 2021, 40(4): 404 (in Chinese)
27 Xiao D H, Liu Y. *Journal of Materials Engineering*[J], 2018, 46(3): 22
28 Han J S, Wu Y Z, Meng J H *et al. Rare Metal Materials and Engineering*[J], 2019, 48(6): 2021
29 Zhang Yang. *Preparation and Properties of (CoNiMgZn)xLi1-xO High Entropy Oxide Ceramics*[D]. Yanshan: Yanshan University, 2022 (in Chinese)
30 Che Jintao. *Study on Microstructure and Mechanical Properties of High Entropy Alloy Containing B*[D]. Guangzhou: Guangdong University of Technology, 2020 (in Chinese)
31 Long Y, Zhang W H, Peng L *et al. Rare Metal Materials and Engineering*[J], 2020, 49(11): 3841
32 Yan Jianhui, Li Kailing, Wang Yi *et al. Materials Reports*[J], 2019, 33(10): 1671 (in Chinese)
33 Ma Siyuan, Guo Qiang, Zhang Di *et al. Materials China*[J], 2019, 38(6): 577 (in Chinese)
34 Wang B J, Wang Q Q, Lu N *et al. Journal of Materials Science & Technology*[J], 2022, 123: 191
35 Raghavendra C R, Basavarajappa S, Irappa S. *Materials Today: Proceedings*[J], 2020, 24: 975
36 Raja R K, Sinha S K. *Materials Chemistry and Physics*[J], 2020, 256: 123709
37 Senkov O N, Senkova S V, Miracle D B *et al. Materials Science and Engineering A*[J], 2013, 565: 51
38 Maiti S, Steurer W. *Acta Materialia*[J], 2016, 106: 87
39 Chen H, Kauffmann A, Laube S *et al. Metallurgical and Materials Transactions A*[J], 2017, 49(3): 772
40 Yao H W, Qiao J W, Gao M C *et al. Materials Science and Engineering A*[J], 2016, 674: 203
41 Zhang Y, Zuo T T, Tang Z *et al. Progress in Materials Science*[J], 2014, 61: 1
42 Chen S, Yang X, Dahmen K *et al. Entropy*[J], 2014, 16(2): 870
43 Qiao D X, Jiang H, Chang X X *et al. Materials Science Forum*[J], 2017, 898: 638
44 Hadraba H, Chlup Z, Dlouhy A *et al. Materials Science and Engineering A*[J], 2017, 689: 252
45 Hadraba H, Chlup Z, Dlouhy A *et al. Intermetallics*[J], 2017, 689: 252
46 Pei Xuhui, Du Yin, Wang Hanming *et al. The Chinese Journal of Nonferrous Metals*[J], 2023, 33: 1 (in Chinese)
47 Chen M, Lan L W, Shi X H *et al. Journal of Alloys and Compounds*[J], 2019, 777: 180

放电等离子烧结WMoNbTaV-Al_2O_3高熵合金组织及磨损性能

刘美君[1]，徐流杰[1,2]，李　洲[1]，郭明宜[1]，胡继康[1]，申华海[3]
(1. 河南科技大学 材料科学与工程学院，河南 洛阳 471000)
(2. 河南科技大学 河南省高温难熔金属材料国际联合实验室，河南 洛阳 471000)
(3. 中国工程物理研究院 核物理与化学研究所，四川 绵阳 621900)

摘　要：以金属粉末为原料，采用放电等离子烧结技术制备新型含α-Al_2O_3的WMoNbTaV难熔高熵合金，研究了烧结温度对合金致密化行为、相结构、显微组织和耐磨性能的影响。结果表明：在1800~1900 ℃烧结时，WMoNbTaV-Al_2O_3高熵合金基体具有单一bcc相结构，Al_2O_3的平均晶粒尺寸为1.15 μm。随着烧结温度升高，合金的晶粒尺寸增大，致密度和显微硬度也在不断增高，在1900 ℃烧结时硬度达到7967.4 MPa。1900 ℃烧结得到的合金具有优异的耐磨性，磨损量仅为1800 ℃烧结合金的一半。且WMoNbTaV-Al_2O_3高熵合金的耐磨性远高于纯W材料。当磨料粒度为37.5 μm时，1900 ℃烧结的合金磨损量为0.9 mg，磨损性能是纯W材料的83倍。

关键词：放电等离子烧结；难熔高熵合金；显微组织；磨损性能

作者简介：刘美君，女，1998年生，硕士生，河南科技大学材料科学与工程学院，河南 洛阳 471000，E-mail：L510522@163.com